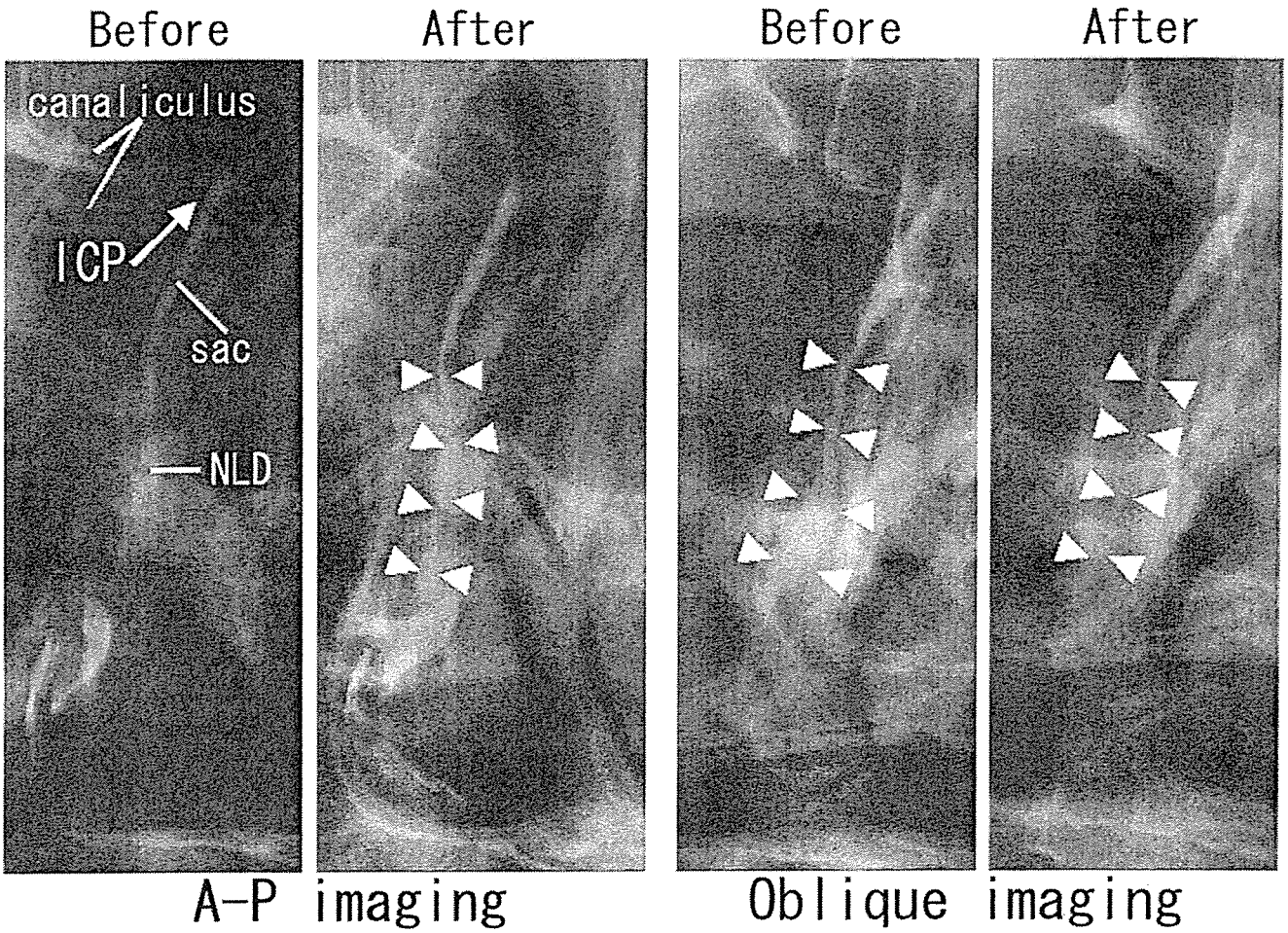

FIGURE 6. Dacryocystography shows reduction of the lumen width of the nasolacrimal drainage system after pilocarpine administration in an anteroposterior (A-P) image and oblique image (arrowheads). ICP = internal common punctum; NLD = nasolacrimal duct.

physiologic characteristics that are similar to those of the nasal mucosa.

Fischer and associates[13] reported that somatostatin and neuropeptide Y (nonadrenergic vasoconstrictors) were present in the human nasal mucosa. Vasoactive intestinal polypeptide and substance P, which are potent mediators of vasodilation, have also been detected in the nasal mucosa.[14] Because some of these peptides are contained in the nasolacrimal drainage system,[2] further investigations on the effect of these peptides on the lumen width of the nasolacrimal drainage system are necessary. The ocular surface and nasal mucosa have sensory innervations, and mechanical[15] and sensory[16] stimulation of the nasal mucosa induces aqueous tear production and vasodilatation of the blood vessels in the nasal mucosa.[17] In addition, the sensitivities of the corneal and conjunctival are correlated with tear clearance.[18] These sensory innervations of the ocular surface and nasal mucosa may play a role in changes of the lumen width of the nasolacrimal drainage system. There are thermoreceptors in the nasal mucosa,[19] and stimulation of these receptors induced a vascular response in the nasal mucosa.[17,20] It is also known that the body surface cooling causes a reflex swelling of the nasal mucosa and that body surface heating induces the shrinkage of the nasal mucosa.[21] These observations indicate that there are many factors that can alter the lumen width of the nasolacrimal system.

Whitnall[4] has shown that the nerves to the LS are derived from the infratrochlear branch of the ophthalmic division of the fifth nerve and that the lower part of the NLD receives axons from the anterior superior alveolar branch of the maxillary division of the same nerve. In addition, the contribution of the seventh cranial nerve, through the Nervus intermedius, to the facial autonomic innervation should be considered.[22–25] The parasympathetic preganglionic fibers arise from the lacrimatory nucleus of the facial nerve, run in the Nervus intermedius of the facial nerve, and then travel in the greater petrosal branch of the nerve. The greater petrosal nerve then joins the deep petrosal nerve to form the nerve of the pterygoid canal. The deep petrosal nerve arises from superior cervical sympathetic ganglion through the internal carotid plexus

and passes without interruption through the pterygopalatine ganglion. Although a detailed map of the innervation of the nasolacrimal drainage system has not been determined, these pathways also may supply innervation to the nasolacrimal drainage system.

A limitation of this study was that we assumed that an increase in the lumen width indicated an increase in the area of the lumen. This assumption would be correct if the lumen was circular, but it is known that the shape of the lumen varies and contains numerous folds and ridges. To test this assumption, we photographed the nasolacrimal drainage system from two directions and measured the width at five different points. The fact that the lumen widths that were obtained with anteroposterior images were not significantly different from those obtained from oblique images would suggest strongly that our assumption was correct. However, additional anatomic studies of the nasolacrimal drainage system will be required to determine the exact relationship between the width and area of the lumen.

Amanat and associates[26] reported that 30% of the patients with unilateral epiphora had a physiologic obstruction in the lower part of the NLD of the asymptomatic side by lacrimal scintigraphy, which indicates that the anatomically asymptomatic side may not be completely physiologically normal in our patients. Even though our use of asymptomatic sides may have introduced some bias to our data, we chose not to use healthy volunteers for ethical reasons. We also believe that a cross-over design with the use of phenylephrine and pilocarpine on the same patient would have increased the statistical power of our conclusions; however, repeated x-ray radiation would have to be performed on the same patient.

The average lumen width of the upper orifice of the osseous NLD is 4.6 mm[4]; the lumen width of the membranous NLD is smaller, because the wall of the membranous NLD becomes thicker in this area.[4,8,9] The lumen width of the LS and the NLD that were measured at the five points tended to be slightly smaller than those reported by Malik and associates[27] (2.43 ± 0.95 mm for the LS, and 2.30 ± 0.83 mm for NLD), who also used dacryocystography with a water-soluble agent. This discrepancy may be because they may have exerted excessive pressure on the LS and NLD by direct insertion of a cannula into the LS, or it may simply reflect racial differences.[28]

It is possible that not using a standardized pressure of infusion of the contrast medium through the canaliculus can lead to artificial distention of the nasolacrimal drainage system on dacryocystography measurements. However, we performed dacryocystography under fluoroscopic guidance and stopped the infusion when the contrast medium was detected in the nasal cavity. In addition, after phenylephrine infusion, 98.0% (50/51) of the lumen width at points 3 through 5 in the anteroposterior images and 94.1% (64/68) at points 2 through 5 in the oblique images were significantly larger. Conversely after pilocarpine infusion, 87.5% (42/48) of the lumen width at points 3 through 5 in anteroposterior images and 96.9% (31/32) at points 4 and 5 in the oblique images were reduced significantly. Moreover, the lumen widths of the LS were not changed significantly, except for one point after phenylephrine infusion. These findings, coupled with our statistical analysis that shows that the changes were statistically significant, indicated that the changes were not due to the injection protocol.

Dacryocystography is the most common and useful method to obtain anatomic information of the nasolacrimal drainage system.[29,30] We selected to use dacryocystography because it is readily available and safe and because the results can be obtained quickly and at low cost.[31–34] Other imaging techniques (e.g., lacrimal scintigraphy,[35] computed tomography,[36,37] and magnetic resonance imaging[29,31,32]) have been used to evaluate the nasolacrimal drainage system. Among these, lacrimal scintigraphy is useful in the evaluation of the physiologic condition of the tear flow dynamics[33,35] but gives limited anatomic information.[33] Conventional computed tomography and magnetic resonance imaging are used to analyze the structure of orbit and the paranasal sinus[33]; however, these procedures cannot distinguish the point of nasolacrimal obstructions precisely.[33,36,37] Although computed tomography dacryocystography provides functional information,[38] a small stenosis or obstruction can be missed between slices.[39] Magnetic resonance dacryocystography is a noninvasive procedure that is used for the functional assessment of the nasolacrimal system.[29,31,32] However, it is expensive, with long image acquisition time, frequent image degradation with patient movement,[32,39] and lower spatial resolution.[29] Helical computed tomography dacryocystography[39] and three-dimensional rotational dacryocystography[40] are new methods for the evaluation of the nasolacrimal drainage system in detail; however, these methods have not yet been established as routine tests and are also expensive.[39] Furthermore, because of the sensitivity, it is difficult often to distinguish between anatomic variations and true filling defects.[39]

O'Donnell and Shah[41] recommended dacryocystorhinostomy (DCR) in cases with a "functional" NLD obstruction and obtained highly successful results after DCR, which suggests a necessity of appropriate lacrimal drainage surgery for this abnormality. This suggested that a dysfunction in the tear outflow in cases of functional NLD obstruction may be attributed to an abnormal autonomic control that reduces tear outflow rather than a weakness of the lacrimal pump. In this respect, the topical application of adrenergic agonist may be useful in the treatment of the functional NLD obstruction. Further studies are necessary to determine the relationship between functional NLD obstruction and the reaction of the nasolacrimal drainage system to adrenergic or cholinergic agonists by topical instillation. In addition, an intentional dilation of the NLD by sympathetic stimulation may be beneficial in the

prevention of the false passage formation at the time of nasolacrimal intubation.

François and Neetens[42] suggested that sensitive receptors were present in the wall of the LS. These receptors would then control tear secretion, because lacrimation can decrease in the absence of inflammation of the LS. Moreover, Yen and associates[43] reported that tear secretion decreased after temporary punctal occlusion in normal subjects, which suggests that there are some receptors on the ocular surface, lacrimal outflow tract, or nasal mucosa that are part of a feedback mechanism that controls tear production. The innervations to the lacrimal gland,[44,45] accessory lacrimal gland,[46,47] meibomian gland,[48] and conjunctival goblet cells[49] have been studied extensively; tear production is believed to be regulated by autonomic and sensory nerves. Earlier, tear outflow was believed to be regulated mainly by the lacrimal pump through the canaliculus and LS that accompanies blinking.[50–54] However, our results suggest that tear outflow may also be affected by changes in the lumen width of the NLD. Because tear fluid contains norepinephrine and epinephrine,[55,56] the innervation of the LS and NLD may be involved actively in this feedback system.

Further studies are needed to determine the relationship between the lumen width in the nasolacrimal drainage system and the kinetics of tear outflow. This is important because these findings are related closely to the differential diagnosis of nasolacrimal stenosis/obstruction and dry eye disorders. The critical question of whether a wide or narrow nasolacrimal drainage system is preferable for smooth tear outflow is now underway.

In summary, our data show that an adrenergic agonist increased the lumen width of the nasolacrimal drainage system, especially the lumen width of the NLD, whereas cholinergic agonist reduced its width. These findings indicate that the drainage of tears through the NLD is controlled, in part at least, by the autonomic nervous system.

REFERENCES

1. Tsuda K. On the histology of ductulus lacrimalis in adults, especially on its innervation. Tohoku J Exp Med 1952;56: 233–243.
2. Paulsen F, Hallmann U, Paulsen J, Thale A. Innervation of the cavernous body of the human efferent tear ducts and function in tear outflow mechanism. J Anat 2000;197:177–187.
3. Paulsen F, Thale A, Hallmann U, Schbaudig U, Tillman B. The cavernous body of the human efferent tear ducts: function in tear outflow mechanism. Invest Ophthalmol Vis Sci 2000;41:965–970.
4. Whitnall SE. The anatomy of the human orbit and accessory organs of vision. 2nd ed. London: Oxford University Press; 1932. Reprinted and published: New York: Robert E. Krieger; 1979, p. 1–252.
5. Tucker NA, Tucker SM, Linberg JV. The anatomy of the common canaliculus. Arch Ophthalmol 1996;114:1231–1234.
6. Schaeffer JP. The nasolacrimal passageways: the nose, paranasal sinus, nasolacrimal passageways, and olfactory organ in man. Philadelphia: P. Blakiston; 1920. p. 237–260.
7. Hoffmann KR, Dmochowski J, Nazareth DP, et al. Vessel size measurements in angiograms: manual measurements. Med Phys 2003;30:681–688.
8. Bailey JH. Surgical anatomy of the lacrimal sac. Am J Ophthalmol 1923;6:665–671.
9. Lang J. Inferior nasal meatus (anatomy of the routes of access). In: Clinical anatomy of the nose, nasal cavity and paranasal sinus. New York: Thieme Medical; 1989. p. 99–102.
10. Änggård A. Parasympathetic control of blood circulation and secretion in the nasal mucosa. Rhinology 1975;13:147–153.
11. Jackson RT. Evidence for presynaptic parasympathetic receptors on nasal blood vessels. Ann Otol Rhinol Laryngol 1982;91:216–219.
12. Olsson P, Bende M. Sympathetic neurogenic control of blood flow in human nasal mucosa. Acta Otolaryngol (Stockh) 1986;102:482–487.
13. Fischer L, Auberson S, Bretton C, Lacroix JS. Adrenergic and non-adrenergic vasoconstrictor mechanisms in the human nasal mucosa. Rhinology 1993;31:11–15.
14. Uddman R, Malm L, Malmö S. Peptide containing nerves in the nasal mucosa. Rhinology 1981;19:75–79.
15. Tsubota K. The importance of the Schirmer test with nasal stimulation. Am J Ophthalmol 1991;111;106–108.
16. Gupta A, Heigle T, Pflugfelder SC. Nasolacrimal stimulation of aqueous tear production. Cornea 1997;16:645–648.
17. Lacroix JS, Potter EK. Nasonasal reflex mechanisms in anaesthetized dogs. Acta Otolaryngol 1999;119:249–256.
18. Afonso AA, Monroy D, Stren ME, et al. Correlation of tear fluorescein clearance and Schirmer test score with ocular irritation symptoms. Ophthalmology 1999;106:803–810.
19. Willatt DJ, Jones AS. The role of the temperature of the nasal lining in the sensation of nasal patency. Clin Otolaryngol 1996;21:519–523.
20. Stangerup SE, Thomsen HK. Histological changes in the nasal mucosa after hot-water irrigation: an animal experimental study. Rhinology 1996;34:14–17.
21. Lundqvist GR, Pedersen OF, Hilberg O, Nielsen B. Nasal reaction to change in whole body temperature. Acta Otolaryngol (Stockh) 1993;113:783–788.
22. Lang J. Innervation of the nasal cavity. In: Clinical anatomy of the nose, nasal cavity and paranasal sinus. New York: Thieme Medical Publishers; 1989. p. 112–116.
23. Snell RS, Lemp MA. The autonomic nervous system. In: Snell RS, Lemp MA, editors. Clinical anatomy of the eye. 2nd ed. Malden (USA): Blackwell Science; 1977. p. 351–378.
24. Ruskell G. Orbital passage of pterygopalatine ganglion efferents to paranasal sinus and nasal mucosa. Cells Tissues Organs 2003;175:223–228.
25. Butler JM, Ruskell GL, Cole DF, et al. Effects of VIIth (facial) nerve degeneration on vasoactive intestinal polypeptide and substance P levels in ocular and orbital tissues of the rabbit. Exp Eye Res 1984;39:523–532.

26. Amanat LA, Hilditch TE, Kwok CS. Lacrimal scintigraphy. III. Physiological aspects of lacrimal drainage. Br J Ophthalmol 1983;67:729–732.
27. Malik SR, Gupta AK, Chaterjee S, Bhardwaj OP, Saha M. Dacryocystography of normal and pathological lacrimal passages. Br J Ophthalmol 1969;53:174–179.
28. Santos-Fernandez J. The measurements of the nasal canal according to the race. Am J Ophthalmol 1921;4:32–37.
29. Yoshikawa T, Hirota S, Sugimura K. Topical contrast-enhanced magnetic resonance dacryocystography. Radiat Med 2000;18: 355–362.
30. Wearne MJ, Pitts J, Frank J, Rose GE. Comparison of dacryocystography and lacrimal scintigraphy in the diagnosis of functional nasolacrimal duct obstruction. Br J Ophthalmol 1999;83:1032–1035.
31. Goldberg RA, Heinz GW, Chiu L. Gadolinium magnetic resonance imaging dacryocystography. Am J Ophthalmol 1993;115:738–741.
32. Hoffmann KT, Hosten N, Anders N, et al. High-resolution conjunctival contrast enhanced MRI dacryocystography. Neuroradiology 1999;41:208–213.
33. Weber AL, Rodriguez-DeVelasquez A, Lucarelli MJ, Cheng HM. Normal anatomy and lesions of the lacrimal sac and duct. Neuroimaging Clin N Am 1996;6:199–217.
34. Hurwitz JJ, Victor WH. The role of sophisticated radiological testing in the assessment and management of epiphora. Ophthalmology 1985;92:407–413.
35. Guzek JP, Ching AS, Hoang TA, et al. Clinical and radiologic lacrimal testing in patients with epiphora. Ophthalmology 1997;104:1875–1881.
36. Russell EJ, Czervionke L, Huckman M, Daniels D, McLachlan D. CT of the inferomedial orbit and the lacrimal drainage apparatus: normal and pathologic anatomy. Am J Roentgenol 1985;145:1147–1154.
37. Groell R, Schaffler GJ, Uggowitzer M, Szolar DH, Muellner K. CT-anatomy of the nasolacrimal sac and duct. Surg Radiol Anat 1997;19:189–191.
38. Saraç K, Hepşen IF, Bayramlar H, Ůguralp M, Toksöz M, Baysal T. Computed tomography dacryocystography. Eur J Radiol 1995;19:128–131.
39. Freitag SK, Woog JJ, Kousoubris PD, Curtin HD. Helical computed tomographic dacryocystography with three-dimensional reconstruction. Ophthal Plast Reconstr Surg 2002;18: 121–132.
40. Lüchtenberg M, Kuhli C, Rochemont RM, et al. Three-dimensional rotational dacryocystography for imaging of the lacrimal draining system and adjacent anatomical structures. Ophthalmologica 2005;219:136–141.
41. O'Donnell B, Shah R. Dacryocystorhinostomy for epiphora in the presence of a patent lacrimal system. Clin Experiment Ophthalmol 2001;29:27–29.
42. François J, Neetens A. Tear flow in man. Am J Ophthalmol 1973;76:351–358.
43. Yen MT, Pflugfelder SC, Feuer WJ. The effect of punctal occlusion on tear production, tear clearance, and ocular surface sensation in normal subjects. Am J Ophthalmol 2001;131:314–323.
44. Seifert P, Stuppi S, Spitznas M, Weihe E. Differential distribution of neuronal markers and neuropeptides in the human lacrimal gland. Graefe's Arch Clin Exp Ophthalmol 1996;234:232–240.
45. Ruskell G. Distribution of pterygopalatine ganglion efferents to the lacrimal gland in man. Exp Eye Res 2004;78:329–335.
46. Seifert P, Stuppi S, Spitznas M. Distribution pattern of nervous tissue and peptidergic nerve fibers in accessory lacrimal glands. Cur Eye Res 1997;16:298–302.
47. Seifert P, Spitznas M. Demonstration of nerve fibers in human accessory lacrimal glands. Graefe's Arch Clin Exp Ophthalmol 1994;232:107–114.
48. Seifert P, Spitznas M. Immunocytochemical and ultrastructural evaluation of the distribution of nervous tissue and neuropeptides in the meibomian gland. Graefe's Arch Clin Exp Ophthalmol 1996;234:648–656.
49. Diebold Y, Ríos JD, Hodges RR, Rawe I, Dartt DA. Presence of nerves and their receptors in mouse and human conjunctival goblet cells. Invest Ophthalmol Vis Sci 2001;42:2270–2282.
50. Jones LT. Epiphora II: its relation to the anatomic structures and surgery of the medial canthal region. Am J Ophthalmol 1957;43:203–212.
51. Jones LT. An anatomical approach to problems of the eyelids and lacrimal apparatus. Arch Ophthalmol 1961;66:111–124.
52. Doane MG. Blinking and the mechanics of the lacrimal drainage system. Ophthalmology 1981;88:844–851.
53. Lemp MA, Weiler HH. How do tears exist? Invest Ophthalmol Vis Sci 1983;24:619–622.
54. Becker BB. Tricompartment model of the lacrimal pump mechanism. Ophthalmology 1992;99:1139–1145.
55. Trope GE, Rumley AG. Catecholamine concentrations in tears. Exp Eye Res 1984;39:247–250.
56. Zubareva TV, Kiseleva ZM. Catecholamine content of the lacrimal fluid of healthy people and glaucoma patients. Ophthalmologica 1977;175:339–344.

Biosketch

Junji Narioka, MD, was educated at Tokushima University School of Medicine in Japan, and has served on the Department of Ophthalmology, Ehime University School of Medicine in Japan. He studied the anatomy of the nasolacrimal drainage system in Division of Anatomy and Embryology at Ehime University School of Medicine in Japan.

Demonstration of Aqueous Streaming Through a Laser Iridotomy Window Against the Corneal Endothelium

Yasuaki Yamamoto, MD; Toshihiko Uno, MD, PhD; Katsumi Shisida, MD; Longquan Xue, MD; Atsushi Shiraishi, MD, PhD; Xiaodong Zheng, MD, PhD; Yuichi Ohashi, MD, PhD

Objective: To determine the pathogenesis of the bullous keratopathy that is frequently observed in patients after argon laser iridotomy (ALI) by comparing the changes in aqueous flow after ALI with those that follow peripheral iridectomy in rabbit eyes.

Methods: Silicone particles were injected into the anterior chamber of rabbit eyes as tracers to monitor aqueous flow. Particle tracking velocimetry with image analysis was used to determine the direction and speed of aqueous flow in 5 pigmented rabbits that underwent ALI and 5 that underwent peripheral iridectomy.

Results: In the ALI group, silicone particles were found to stream through the iridotomy window against the corneal endothelium immediately after the pupil was constricted by a light stimulus. The mean±SD speed of the particles was 2.97±1.51 mm/s. In contrast, the mean±SD flow rate through the iridectomy window in the peripheral iridectomy group was significantly slower at 0.36±0.30 mm/s (P=.01).

Conclusion: Constriction of the pupil elicited marked aqueous streaming through the ALI window against the corneal endothelium.

Clinical Relevance: The mechanical stress to the corneal endothelium by the abnormal aqueous stream may be partially responsible for the corneal decompensation that follows ALI.

Arch Ophthalmol. 2006;124:387-393

ARGON LASER IRIDOTOMY (ALI) has been widely used for the prevention and treatment of angle closure glaucoma since its introduction into clinical practice by Quigley[1] in 1981. In 1984, Pollack[2] reported the first case of irreversible corneal edema after ALI, and in 1988, Schwartz et al[3] reported more cases of phakic bullous keratopathy and concluded that corneal edema was a serious complication of ALI. The incidence of this devastating disorder is increasing yearly, and, in Japan, ALI-induced bullous keratopathy is now recognized as the second most common corneal disease requiring penetrating keratoplasty to restore good visual acuity.[2-11]

A variety of causes have been postulated for bullous keratopathy, for example, excessive laser irradiation,[3,4,7-9,11] a history of acute glaucomatous attack,[3,5,6,8,10,11] diabetes mellitus,[3,6,8,11] and abnormalities in the corneal endothelium, such as cornea guttata and Fuchs corneal degeneration.[3,6,7-9,11] However, these factors do not fully explain the pathogenetic mechanism in most cases.

We hypothesize that changes in the dynamics of the flow of aqueous humor are related to the corneal endothelial decompensation that follows ALI. To date, the dynamic changes in aqueous flow in the anterior chamber have not been studied in detail because aqueous flow is not visible except when inflammatory cells are present in the anterior chamber. Recent improvements in imaging devices and computer techniques now allow the use of principles developed for particle tracking velocimetry (PTV) to detect the flow of the aqueous humor.[12,13] Using silicone powder as a tracer, we quantitatively analyzed changes in the direction and speed of aqueous flow and compared the velocity and course of aqueous flow after ALI vs after peripheral iridectomy (PI) in rabbits.

Author Affiliations:
Departments of Ophthalmology, Ehime University, Shitsukawa, Toon-city, Ehime (Drs Yamamoto, Uno, Shisida, Xue, Shiraishi, Zheng, and Ohashi), and Takanoko Hospital, Matsuyama City (Drs Yamamoto and Shiraishi), Japan.

METHODS

ANIMALS AND TRACER

Healthy Dutch pigmented rabbits (weight, 1.5-2.5 kg) were used. All the procedures were performed under general anesthesia with an intramuscular injection of 5% ketamine

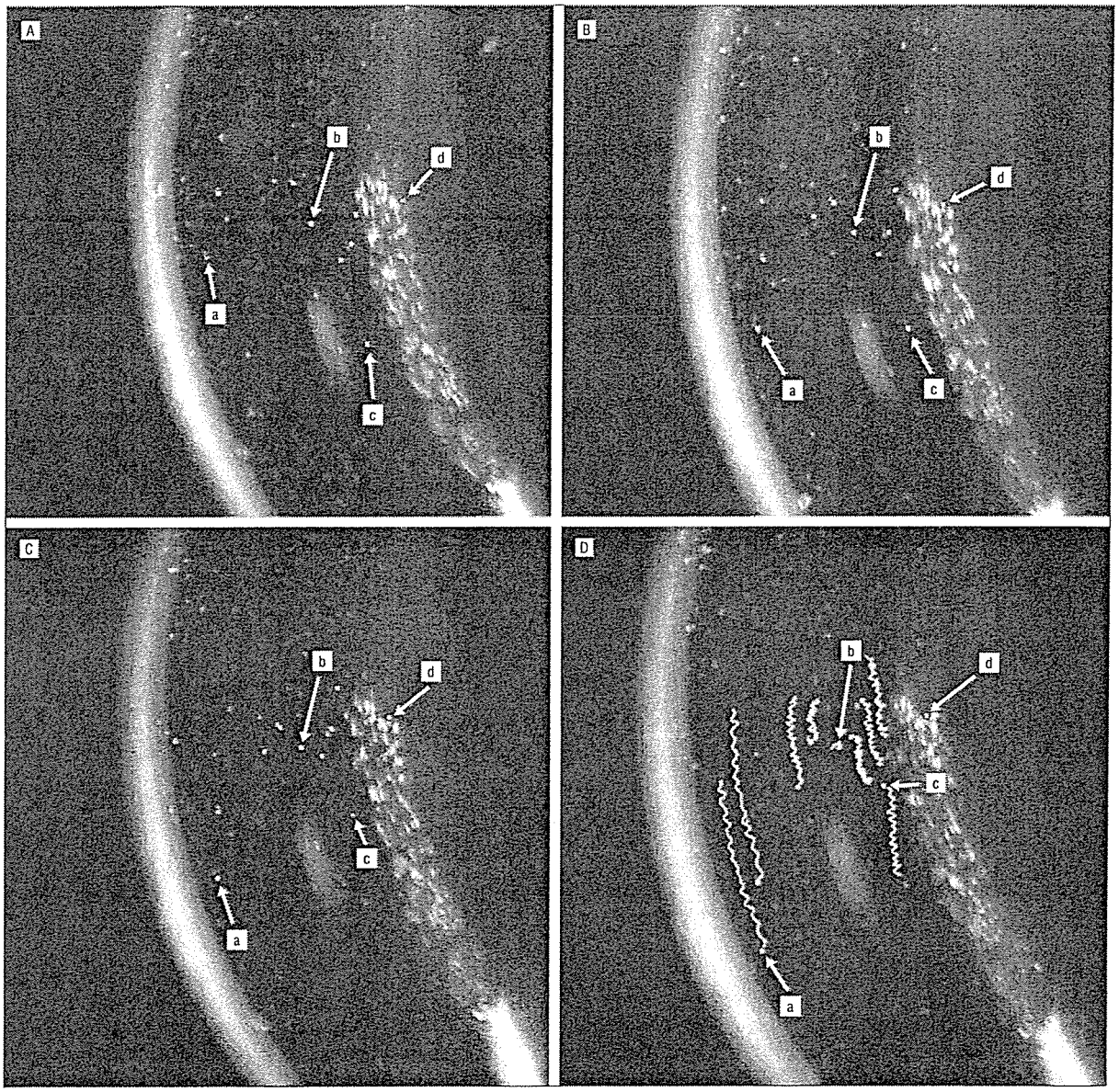

Figure 1. Still photographs of particles in the anterior chamber at 0 (A), 3 (B), 5 (C), and 8 (D) seconds showing a descending particle (a), the center of the circular current (b), and an ascending particle (c). Particles attached to the surface of the lens are used to track the movement of the rabbit (d). The wavy lines in D indicate the track of each particle.

hydrochloride, 25 mg/kg (Ketalar; Sankyo-Yell, Tokyo, Japan), and xylazine hydrochloride, 5 mg/kg (Celactar; Bayer, Tokyo), and under topical corneal anesthesia with 0.4% oxybuprocaine hydrochloride ophthalmic solution. In managing the rabbits, we adhered strictly to the Guiding Principles in the Care and Use of Animals (US Department of Health, Education, and Welfare publication NIH 80-23).

Silicone powder (KMP-602; Shin-Etsu Chemical Co Ltd, Tokyo), consisting of homogeneous particles with a mean diameter of 30 μm and specific gravity of 0.98, was used as a tracer to make aqueous flow visible.

EXPERIMENTAL DESIGN

Fifteen rabbits were randomly separated into 3 equal groups. One group served as controls without treatment, the second group underwent unilateral ALI, and the third group underwent unilateral PI. The rabbits in the ALI and PI groups were monitored for more than 2 weeks until the inflammatory reactions induced by the surgical procedures were completely resolved.

To examine the pattern and velocity of aqueous flow, 0.05 g of silicone powder was suspended in 10 mL of isotonic sodium chloride solution. Then, 0.2 mL of the suspension was injected through a corneal limbal incision at the 2-o'clock position using a 30-gauge needle on a 1-mL disposable syringe. All the rabbits were allowed to recover for at least 15 minutes after the injection, until the movements of the silicone particles became consistent. Then, the movements of the silicone particles were videotaped and analyzed using PTV.

In the control group, the speed of the thermal current was quantitatively analyzed, and in the ALI and PI groups, the movement of the tracer particles in the vicinity of the iridotomy or

iridectomy window was also measured. To induce pupillary constriction, the width of the slit beam was increased from 0.3 to 2.0 mm. Changes in aqueous flow were monitored before and during miosis. The speed of flow of the aqueous from the posterior chamber through the opening in the iris into the anterior chamber was compared in the 2 groups.

EXAMINATION OF AQUEOUS FLOW AND PTV

Movement of the silicone particles into the anterior chamber was observed by using a slitlamp biomicroscope and was recorded on videotape by using a charge-coupled device camera. The slit beam was aligned with the center of the cornea and projected vertically onto the anterior surface of the lens. The angle between the observer's eye and the slit beam was maintained at 60°.

The images of the movement of the particles on the videotape were transferred to a personal computer, and the flow speed was determined by monitoring the displacement of individual particles using image analysis software (Image Tracker PTV 2001; Digimo Co Ltd, Osaka, Japan). The images were first converted into still pictures at 30 frames per second, and the coordinates of selected particles were determined for each frame. Then, regression lines were calculated based on the sequential changes of the coordinates of each particle. The speed of flow of the particles was calculated from the slope of each regression line.

Because the coordinates of the particles also changed from movements of the rabbit, the coordinates of each particle were corrected by subtracting the coordinates of particles that were adherent to the surface of the lens or corneal endothelium from those of the individual particles floating in the aqueous humor.

SURGICAL PROCEDURES FOR ALI AND PI

The multicolor laser photocoagulater (Novus Omni; Coherent, Inc, Santa Clara, Calif) was used for ALI. The 2-step long-burn technique using the Abraham lens was used: 8 stretching burns with 521 nm of argon green, 200-μm spot size, 0.2 second, and 200 mW of power followed by 272 to 432 penetrating burns with 521 nm of argon green, 50-μm spot size, 0.02 second, and 1000 mW of power. For PI, the iris was pulled out of a limbal incision and resected to produce an iridectomy diameter of approximately 3.0 mm at the 12-o'clock position. The prolapsed iris was gently repositioned using a spatula to avoid any incarceration in the incision site. Finally, the wound was closed using a single 10-0 nylon suture.

RESULTS

The silicone particles were well dispersed in the aqueous humor without any aggregation. Some particles were adherent to the corneal endothelium and the anterior surface of the lens and iris, but most were seen to be moving along with the aqueous flow.

AQUEOUS FLOW IN THE ANTERIOR CHAMBER

Control Group

Slitlamp examination showed continuous movement of the particles in a circular path, with a descending flow near the corneal endothelium and an ascending flow near the anterior surface of the iris. This pattern is consistent with the theory of the thermal current of the aqueous humor in the anterior chamber[14] (**Figure 1**). Changes in the coordinates of 19 particles in 5 rabbit eyes were plotted. The graph of 1 descending particle in the vicinity of the corneal endothelium is shown in **Figure 2**. The mean±SD flow speeds were 0.180±0.056 mm/s for the descending flow near the corneal endothelium and 0.068±0.015 mm/s for the ascending flow near the anterior surface of the lens.

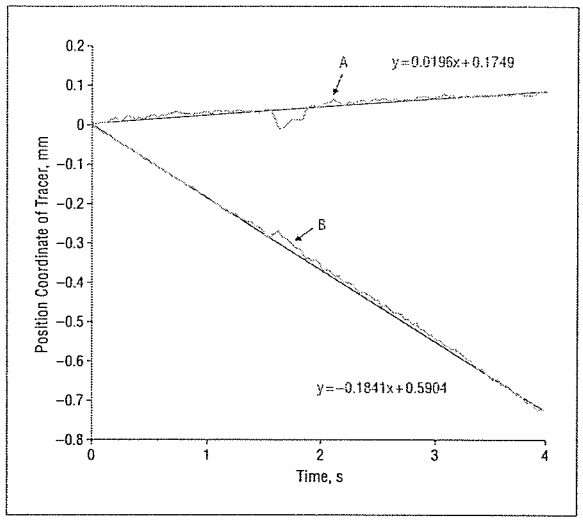

Figure 2. Changes in the coordinates of the movement of 1 descending particle in the vicinity of the corneal endothelium. Position "0" represents the starting position of the particle in the anterior chamber. A shows the changes in the coordinates from the cornea to the iris. B represents the particle position from top to bottom. Flow speed is calculated from the slope of the regression line.

ALI Group

The pattern of thermal flow of the particles was almost the same as in control eyes. However, when the pupil was constricted, a stream of particles was seen to flow into the anterior chamber from the posterior chamber through the iridotomy window. After the pupil dilated, the particles were drawn back into the posterior chamber through the iridotomy window. The tracking images of these particles, plotted by monitoring individual particles for 1 second, are shown in **Figure 3** and **Figure 4**. The streaming particles were seen to collide against the corneal endothelium and then move downward in the anterior chamber (arrows in Figure 3).

PI Group

In the PI group, particles were seen to descend not only near the cornea but also along the anterior surface of the lens. The ascending particles were seen near the surface of the iris when the slit beam was shifted laterally. Constriction of the pupil accelerated the speed of the descending particles near the iridectomy window to some extent, but no particles were seen to collide with the corneal endothelium. The tracking images of these particles, plotted for 1 second, are shown in **Figure 5**.

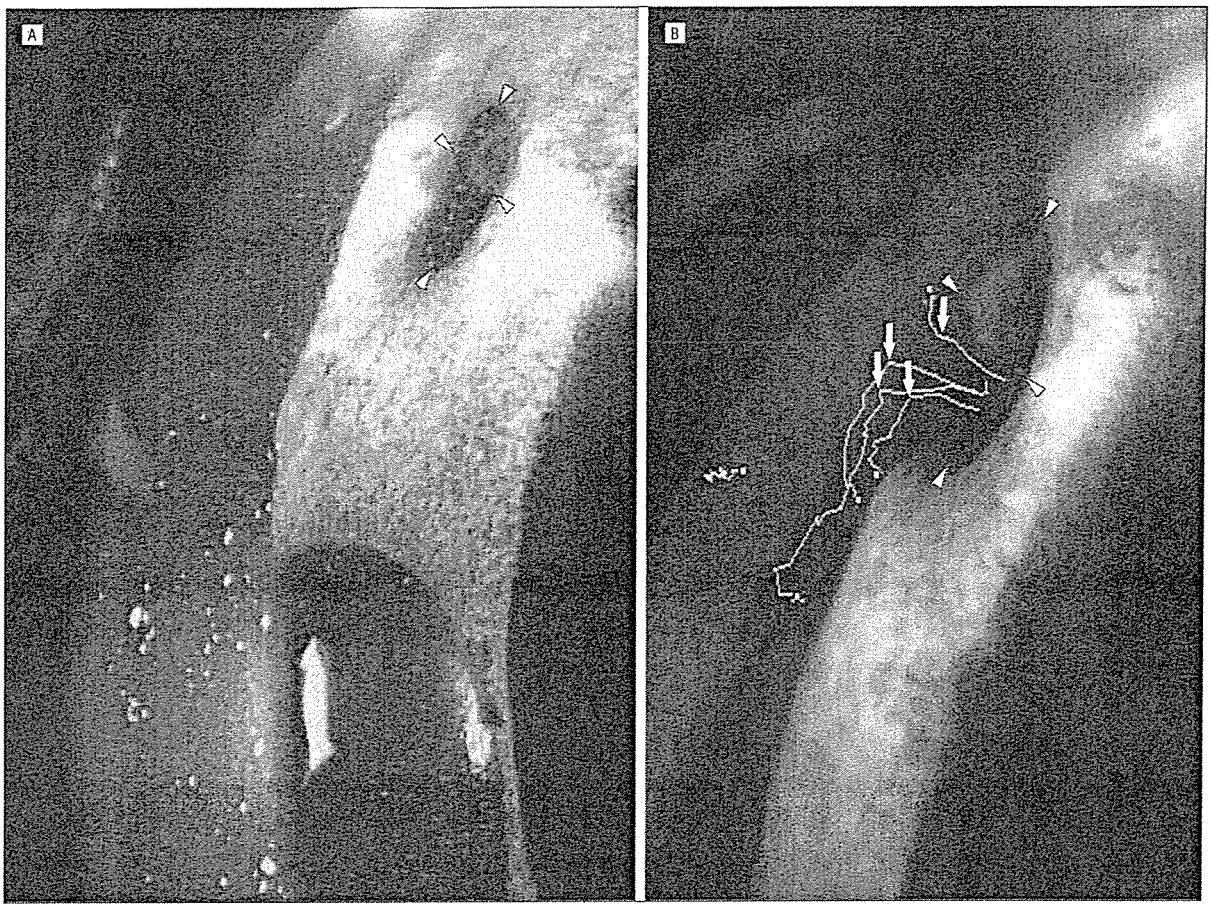

Figure 3. Photograph demonstrating aqueous streaming into the anterior chamber from the posterior chamber through the argon laser iridotomy (ALI) window. A, An eye with ALI during pupil constriction (when the slit beam was increased). B, At that time, the tracking images of streaming particles are indicated in the higher view of the vicinity of the iridotomy window (arrowheads). The particles collided against the corneal endothelium (arrows). The wavy lines indicate the track of each particle.

COMPARISON OF FLOW THROUGH THE OPEN WINDOW IN THE IRIS AFTER MIOSIS IN BOTH GROUPS

The speed of the particles streaming through the opening in the ALI and PI group during a 0.1-second period after miosis is plotted in **Figure 6**. The mean±SD flow speed of the 25 particles in the ALI group was 2.97±1.51 mm/s, whereas that of the 25 particles in the PI group was 0.36±0.30 mm/s. This difference in the mean flow speed was significant ($P=.01$, by Mann-Whitney test). The size of the iris window was measured on the images downloaded to the computer. The mean±SD area of laser iridotomy in the ALI group was 0.96±0.31 mm^2, whereas that in the PI group was 5.84±2.12 mm^2. The difference in the areas of the iris window between the 2 groups was significant ($P=.006$, by Mann-Whitney test).

COMMENT

We succeeded in "seeing" the flow of aqueous humor in the anterior chamber of rabbit eyes by using silicone powder as a tracer. The technique of PTV was then used to determine the direction and speed of the particles. Our results confirm the presence of a thermal current of aqueous humor in the anterior chamber. As stated, the accuracy of the velocity measurement by PTV is ultimately determined by the ability of the scattering particles to follow the instantaneous motion of the fluid.

In this sense, careful selection of a tracer particle is critical, and several properties should be present in the particles. First, the tracer particles must be large enough to have good light-scattering ability and to be detected by a video camera so that digitized data can be analyzed. Second, the tracer particle should be small enough to be carried passively with the current of the fluid. An ideal tracer particle would have a specific gravity identical to that of the aqueous humor. And third, the particle should be nontoxic, noncorrosive, and chemically inert. With respect to these requirements, many studies have used particles with diameters ranging from 2 to 500 μm and density ratios of 0.7 to 1.05.[15] Silicone powder has these properties and thus was used in this study.

The exact cause of the corneal endothelial decompensation that follows ALI has not been determined. For example, excessive laser irradiation can cause serious endothelial damage, but we seldom see such a

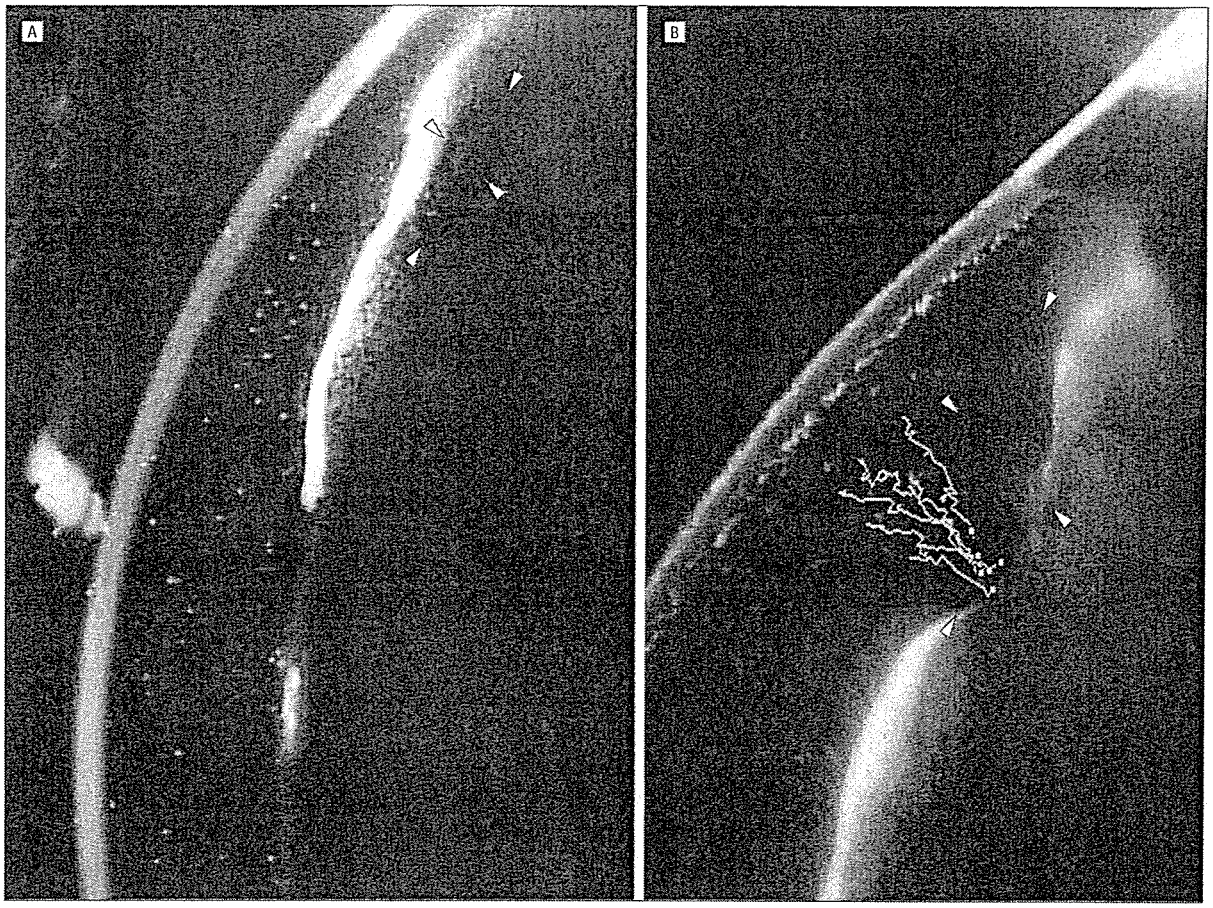

Figure 4. Photograph demonstrating the drawn-back flow into the posterior chamber through the argon laser iridotomy (ALI) window. A, An eye with ALI during dilation of the pupil (when the slit beam was narrowed). B, At that time, the tracking images of particles flow back into the posterior chamber and are indicated by the higher view in the vicinity of the iridotomy window (arrowheads). The wavy lines indicate the track of each particle.

patient develop severe corneal edema immediately after surgery. In addition, corneal endothelial decompensation can develop even after uneventful laser procedures. Although a history of acute glaucomatous attack is a risk factor for corneal endothelial decompensation, irreversible bullous keratopathy almost never develops in eyes that undergo surgical iridectomy. The presence of diabetes mellitus or corneal endothelial abnormalities, such as cornea guttata or Fuchs corneal dystrophy, has not been associated with many cases of bullous keratopathy.

Our most striking finding was the presence of aqueous streaming through the small opening of the iris after ALI. This showed that laser iridotomy causes an extremely fast forward aqueous flow, which occurs through the iris window during miosis, followed by the backward flow as the pupil dilates. The mean speed of this streaming from the posterior chamber to the anterior chamber was estimated to be 2.97 mm/s, which is approximately 17 times faster than the ordinary thermal current. More important, the stream was directed against the corneal endothelium, unlike the direction of the physiologic thermal current, which flows parallel to the corneal endothelium. Just as the continuous shear stress of vascular flow on vascular endothelial cells has gained attention as a causative mechanism in arteriosclerosis or aneurysm formation,[16-18] such an abnormal stream can be suggested to damage corneal endothelial cells. If this streaming is repeated in response to light stimuli for long periods, the corneal endothelial cells around the window may be damaged, leading to corneal endothelial cell dysfunction.

In contrast to the stream observed in the ALI group, the flow speed through a large-diameter surgical iridectomy in the PI group was found to be slow and not directed against the corneal endothelium. This may explain the fewer cases of endothelial dysfunction observed in patients after standard surgical PI, a procedure widely performed before the development of ALI.

Corneal endothelial dysfunction occurs predominantly after ALI but also rarely after Nd:YAG laser iridotomy. One may argue that such corneal endothelial decompensation can be avoided if an Nd:YAG laser is applied to make an iris opening because the thermal effect is thought to be substantially reduced using this procedure. However, it has been reported that the dysfunction can develop in patients after laser iridotomy using an Nd:YAG laser.[7,9,19,20] Therefore, it seems that the thermal damage to the corneal endothelium elicited by the ALI procedure cannot be the only causative factor, and

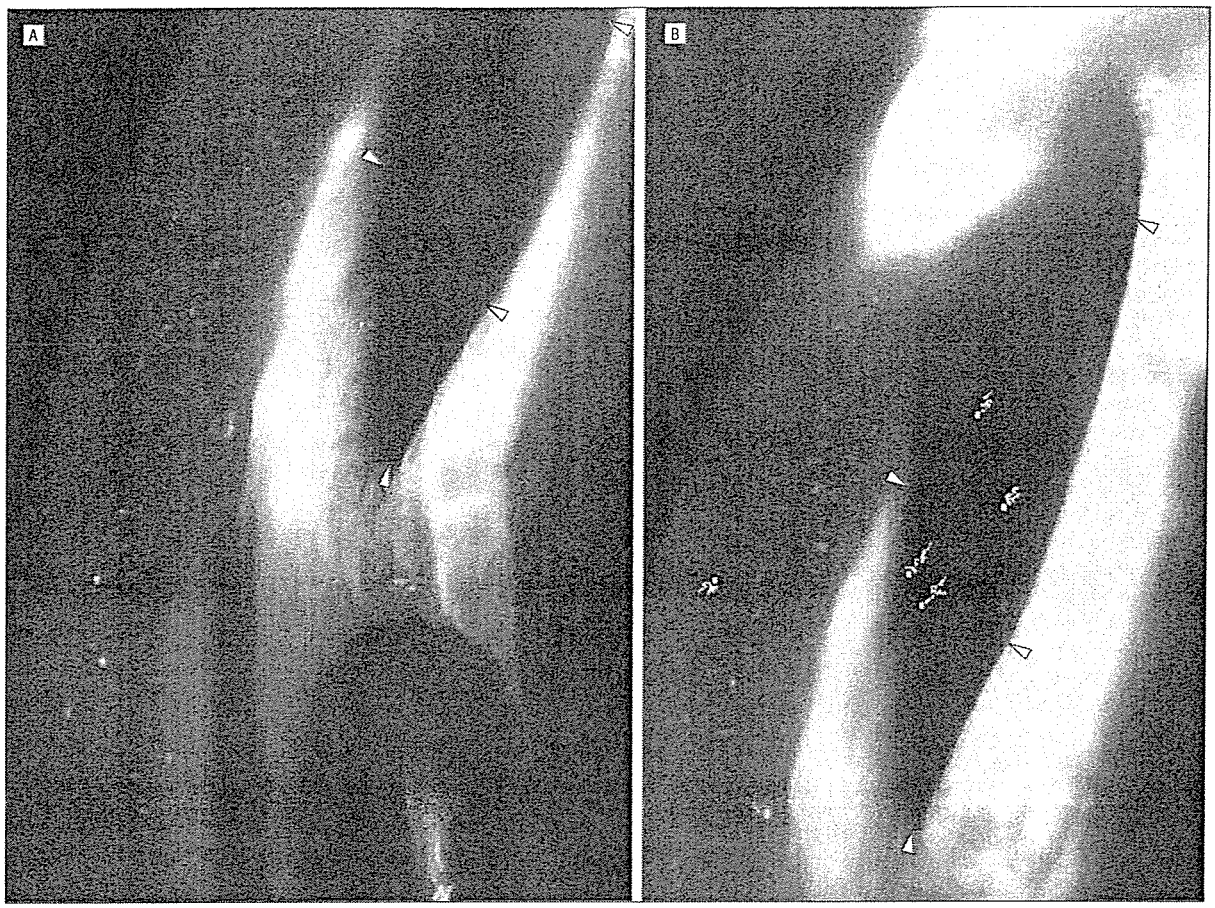

Figure 5. Photograph demonstrating the aqueous flow through the peripheral iridectomy (PI) window. A, An eye with PI during pupil constriction (when the slit beam was increased). B, At that time, the tracking images of particles are indicated by the higher view in the vicinity of the iridectomy window (arrowheads). None of the particles were noted to collide with the corneal endothelium. The wavy lines indicate the track of each particle.

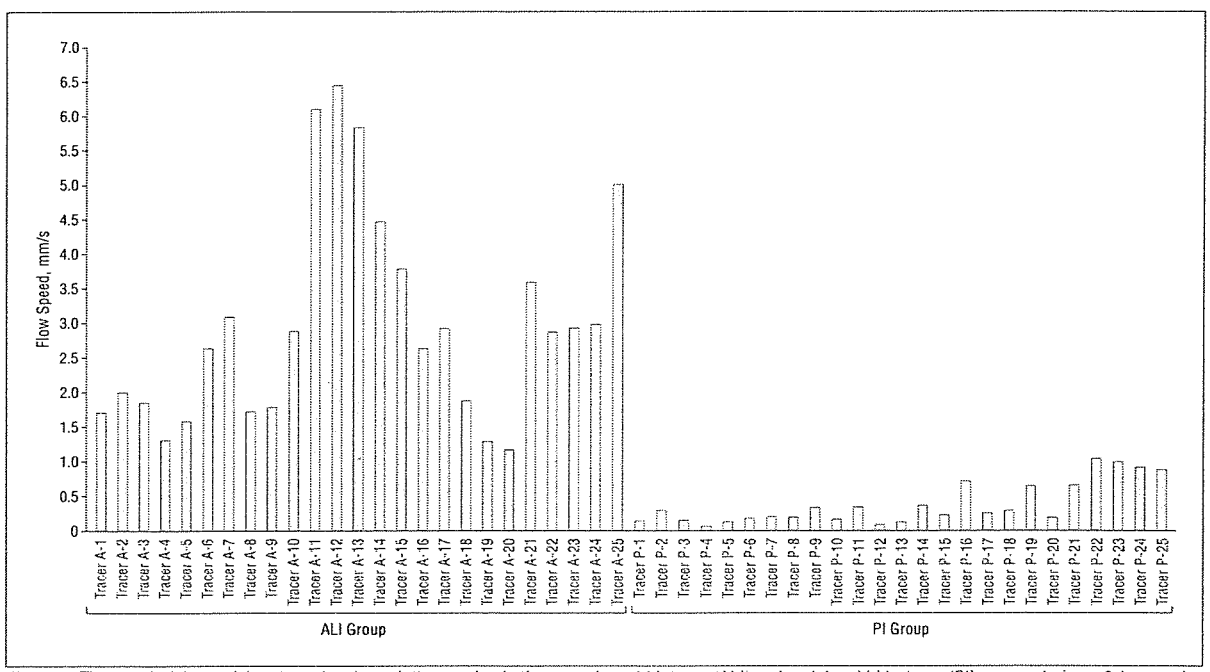

Figure 6. The speed of the particles streaming through the opening in the argon laser iridotomy (ALI) and peripheral iridectomy (PI) groups during a 0.1-second period after miosis. The mean±SD flow speed in the ALI group was 2.97±1.51 mm/s and in the PI group was 0.36±0.30 mm/s (P=.01, by Mann-Whitney test).

the importance of the changes in aqueous flow should be considered.

This type of unusual streaming should be present in all patients to some degree; however, corneal endothelial dysfunction develops in few patients. Possible explanations for this discrepancy include differences in the size of the iridotomy, the location of the window, the distance between the window and the corneal endothelium, and the presence or absence of posterior synechia. These factors are intricately intertwined, and few patients will experience serious corneal endothelial dysfunction that leads to irreversible bullous keratopathy.

Why does such streaming occur? Generally, during miosis, the pressure in the posterior chamber rises, which leads to the flow of aqueous into the anterior chamber. As the pupil and the central region of the posterior surface of the iris make appositional contact with the anterior surface of the lens and retard aqueous flow, the rapid release of the pressure should result in the aqueous stream when the opening is small.

Because the aqueous humor plays an essential role in maintaining the homeostasis of the anterior segment of the eye, any changes may have a profound effect and could be associated with a variety of ocular disorders. In this regard, the method of making aqueous flow visible described herein can be used to analyze changes in its dynamics and could possibly contribute to the further understanding of the pathogenesis of anterior segment disorders.

Submitted for Publication: April 20, 2005; accepted July 15, 2005.
Correspondence: Yasuaki Yamamoto, MD, Department of Ophthalmology, Ehime University, Shitsukawa, Toon-city, Ehime, Japan (yyasuaki@m.ehime-u.ac.jp).
Financial Disclosure: None.

REFERENCES

1. Quigley HA. Long-term follow-up of laser iridotomy. *Ophthalmology.* 1981;88:218-224.
2. Pollack IP. Current concepts in laser iridotomy. *Int Ophthalmol Clin.* 1984;24:153-180.
3. Schwartz AL, Martin NF, Weber PA. Corneal decompensation after argon laser iridectomy. *Arch Ophthalmol.* 1988;106:1572-1574.
4. Hong C, Kitazawa Y, Tanishima T. Influence of argon laser treatment of glaucoma on corneal endothelium. *Jpn J Ophthalmol.* 1983;27:567-574.
5. Zabel RW, MacDonald IM, Minstsioulis G. Corneal endothelial decompensation after argon laser iridotomy. *Can J Ophthalmol.* 1991;26:367-373.
6. Jeng S, Lee JS, Haung SCM. Corneal decompensation after argon laser iridotomy: a delayed complication. *Ophthalmic Surg.* 1991;22:565-569.
7. Wilhelmus KR. Corneal edema following argon laser iridotomy. *Ophthalmic Surg.* 1992;23:533-538.
8. Yuguchi M, Nagasaka M. Bullous keratopathy following argon laser iridotomy. *Jpn J Clin Ophthalmol.* 1992;86:2098-2101.
9. Hosotani H, Ohashi Y, Ohguro N, Kuwayama Y, Knoshita S. Corneal endothelial decompensation after argon laser iridotomy. *Jpn J Clin Ophthalmol.* 1994; 48:420-422.
10. Ishimura H, Kono M, Nakamura J. Bullous keratopathy following argon laser iridotomy. *Jpn J Clin Ophthalmol.* 1997;51:1123-1126.
11. Kanai H, Sotozono C, Komuro A, et al. Bullous keratopathy following argon laser iridotomy. *Atarashii Ganka.* 2003;20:245-249.
12. Adrian RJ. Particle-imaging techniques for experimental fluid mechanics. *Annu Rev Fluid Mech.* 1991;23:261-304.
13. Adrian RJ. Bibliography of particle velocimetry using imaging methods. *TAM Rep.* 1996;817:1917-1995.
14. Duke-Elder S, Gloster J, Weale R. The circulation of the aqueous humour. In: *Physiology of the Eye and of Vision.* St Louis, Mo: CV Mosby; 1968;V:118-130.
15. Melling A. Tracer particles and seeding for particle image velocimetry. *Meas Sci Technol.* 1997;8:1406-1416.
16. Ku DN, Giddens DP, Zarins CK, Glagov S. Pulsatile flow and atherosclerosis in the human carotid bifurcation. *Arteriosclerosis.* 1985;5:293-301.
17. Nerem RM, Harrison DG, Taylor WR, Alexander RW. Hemodynamics and vascular endothelial biology. *J Cardiovasc Pharmacol.* 1993;21:S6-S10.
18. Ujiie H, Tachibana H, Kajiya F, et al. Effect of size and shape (aspect ratio) on the hemodynamics of saccular aneurysms: a possible index for surgical treatment of intracranial aneurysms. *Neurosurgery.* 1999;45:119-130.
19. Panek WC, Lee DA, Christensen RE. The effects of Nd:YAG laser iridotomy on the corneal endothelium. *Am J Ophthalmol.* 1991;111:505-507.
20. Wu SC, Jeng S, Huang SCM, Lin SM. Corneal endothelial damage after neodymium: YAG laser iridotomy. *Ophthalmic Surg Lasers.* 2000;31:411-416.

Current Eye Research, 31:129–136, 2006
Copyright © Taylor & Francis Group, LLC
ISSN: 0271-3683 print / 1460-2202 online
DOI: 10.1080/02713680500507200

Taylor & Francis
Taylor & Francis Group

Role of Angiotensin II Receptor Subtypes in Conjunctival Wound Healing

Shiro Mizoue
Department of Ophthalmology, and Department of Molecular and Cellular Biology, Division of Medical Biochemistry and Cardiovascular Biology, Ehime University School of Medicine, Ehime, Japan

Masaru Iwai, Ayumi Ide, Jun Suzuki, and Masatsugu Horiuchi
Department of Molecular and Cellular Biology, Division of Medical Biochemistry and Cardiovascular Biology, Ehime University School of Medicine, Ehime, Japan

Atsushi Shiraishi and Yuichi Ohashi
Department of Ophthalmology, Ehime University School of Medicine, Ehime, Japan

ABSTRACT *Purpose*: To investigate the role of angiotensin II (Ang II) receptor subtypes in subconjunctival injury. *Methods*: A wound-healing model was developed by subconjunctival blunt dissection in male wild-type, AT_{1a} receptor–deficient ($AT_{1a}KO$) and AT_2 receptor–deficient (AT_2KO) mice. Collagen deposition and cell infiltration were evaluated histologically. Expression of collagen, matrix metalloproteinase (MMP), and tissue inhibitor of metalloproteinase-1 (TIMP-1) were determined by real-time PCR. *Results*: Subconjunctival injury increased the infiltration of inflammatory cells, collagen deposition in the subconjunctival space, and the expression of collagen type I and type III, TIMP-1 and MMP2. In $AT_{1a}KO$ mice, collagen deposition, cell infiltration, and expression of collagen and TIMP-1 were inhibited, but MMP2 expression was enhanced. In contrast, in AT_2KO mice, the increase in collagen deposition, cell infiltration, and expression of collagen and TIMP-1 were further enhanced. *Conclusions*: These results indicate that AT_{1a} and AT_2 receptor stimulation may in addition to other mechanisms be antagonistically involved in the wound-healing process after subconjunctival injury.

KEYWORDS angiotensin II; collagen; conjunctiva; transgenic mouse; wound healing

INTRODUCTION

The conjunctival wound-healing reaction seems to play a key role in the results of surgery for glaucoma[1] or pterygium[2] and ocular surface reconstruction.[3] However, the mechanism of the conjunctival wound-healing reaction has not been fully elucidated despite its clinical importance.

Angiotensin II (Ang II) regulates wound healing in the skin, as well as cardiovascular structure and hemodynamics, through type 1 (AT_1) and type 2 (AT_2) receptors.[4–7] Fibroblasts and phenotypically transformed myofibroblasts[8] play a critical role in cardiac remodeling through extracellular matrix (ECM) protein deposition and both matrix metalloproteinase (MMP) and tissue inhibitor of metalloproteinase-1 (TIMP-1) production.[9] It has been reported that AT_1 receptor stimulation induces cell proliferation and accumulation of ECM.[4] On the other hand, AT_2 receptor stimulation has shown antagonistic actions against AT_1 receptor stimulation in various experiments.[4,10,11] Because it is reported that both AT_1 and AT_2 receptors are expressed in the eye,[12] it seems probable that these receptors play a critical role in the wound-healing process in ocular

Received 24 August 2004
Accepted 15 February 2005

Correspondence: Masatsugu Horiuchi, M.D., Ph.D., Department of Molecular and Cellular Biology, Division of Medical Biochemistry and Cardiovascular Biology, Ehime University School of Medicine, Shitsukawa, Shigenobu, Onsen-gun, Ehime 791-0295, Japan. E-mail: horiuchi@m.ehime-u.ac.jp

tissue. However, the mechanism of action of AT_1 and AT_2 receptor stimulation is unknown.

In the current study, we developed a subconjunctival wound-healing model using Ang II receptor–deficient mice and examined the role of Ang II in subconjunctival wound-healing responses.

MATERIALS AND METHODS

Animals

Adult male C57BL/6J mice (WT), AT_{1a} receptor–deficient (AT_{1a}KO) mice (based on C57BL/6J strain and donated by Tanabe Seiyaku Co. Ltd., Osaka, Japan), and AT_2 receptor–deficient (AT_2KO) mice (based on C57BL/6J strain) (10 to 12 weeks of age) were used in this study. The animals were housed in a room where lighting was controlled (12 hr on, 12 hr off) and the temperature was maintained at 25°C. They were given a standard diet and water *ad libitum*. All experiments were approved by the Animal Studies Committee of Ehime University.

Surgical Procedure

All experimental procedures were carried out in accordance with the Declaration of Helsinki and the Guiding Principles in the Care and Use of Animals (DHEW Publication, NIH 80-23). The surgical procedure was performed under a microscope (OPMI-1SH; Carl Zeiss Inc., Oberkochen, Germany), according to the method of Reichel et al.[13] with slight modification. The mice were anesthetized with ketamine (70 mg/kg) and xylazine (4 mg/kg) by intraperitoneal injection. The upper and lower eyelids were retracted with a small speculum. A small radial incision was made with vannas scissors at a location 1 mm posterior to the corneal limbus. An Obstbaum IOL spatula (ASICO LLC, Westmont, IL, USA) was inserted into the incision and the anterior subconjunctiva was dissected bluntly from the corneal limbus to the fornix. Sham operation was performed without dissecting the subconjunctival area. After surgery, ointment containing antibiotics was applied once on the incision to reduce the risk of infection. Animals were sacrificed at 0.5, 1, 2, 7, and 14 days after surgery with an overdose of pentobarbital. We used 4 to 6 animals for histological analysis, and 6 to 9 animals for measurement of mRNA by real-time PCR in each experimental group.

Histological Examination

The eyes were enucleated and postfixed in 10% neutral buffered formalin overnight, dehydrated, and embedded in paraffin. Then, 5-μm-thick sections were prepared in the pupil–optic nerve head plane. Hematoxylin and eosin staining and Elastica van Gieson staining were carried out to examine cell infiltration and fibrosis in the subconjunctival space. The number of infiltrated cells in the subconjunctival space was counted using the computer software Personal Image Version 3.0 for Windows (ATTO Co., Tokyo, Japan) by investigators who were masked to the treatment and was expressed as the number of nuclei per field (magnification, ×400). We calculated cell number in two microscopic fields from each animal using three different sections from each eye sample. Intensity of fibrosis was graded as follows: 0, negative; 1, weak; 2, moderate; and 3, strong; and was evaluated in three different sections for each animal. Fibrosis score was expressed as mean ±SEM of scores in experimental groups.

Immunohistochemical staining of macrophages and myofibroblasts was performed using a biotin-conjugated secondary antibody (DakoCytomation Japan, Tokyo, Japan) and streptavidin-biotin-peroxidase technique. Cy3- and FITC-conjugated streptavidin (KPL, Inc., Gaithersburg, MD, USA, and Vector Laboratories, Inc., Burlingame, CA, USA, respectively) were used for double staining of AT_1 and AT_2 receptors. Macrophages (F4/80), AT_1 receptor, and AT_2 receptor were stained with anti-F4/80 antibody (BMA Biomedicals, August, Switzerland), anti-AT_1 receptor antibody (Santa Cruz Biotechnology, Santa Cruz, CA, USA), and anti-AT_2 receptor antibody (Santa Cruz Biotechnology), respectively. Immunostaining of α-smooth muscle (α-SM) actin was performed with anti-α-SM actin monoclonal antibody (clone no. 1A4, Sigma-Aldrich, St. Louis, MO, USA) using a mouse-on-mouse reagent (M.O.M. Immuno Detection Kit; Vector Laboratories).

Real-Time PCR

Total RNA was extracted from the conjunctiva and injured subconjunctival tissue using an RNeasy kit (Qiagen Inc., Valencia, CA, USA). Equal amounts of total RNA were reverse-transcribed to cDNA using Omniscript Reverse Transcription Reagents (Qiagen Inc.) according to the manufacturer's protocol. PCR primers

TABLE 1 Primer Sequences for Real-Time PCR

Primer	Sequence
Collagen type I	
Forward	5′-CCGTGCTTCTCAGAACATCA-3′
Reverse	5′-GAGCAGCCATCGACTAGGAC-3′
Collagen type III	
Forward	5′-GTCCACGAGGTGACAAAGGT-3′
Reverse	5′-GATGCCCACTTGTTCCATCT-3′
TIMP-1	
Forward	5′-AGACCACCTTATACCAGCGT-3′
Reverse	5′-TAAACAGGGAAACACTGTGC-3′
MMP1	
Forward	5′-CTCACAACAATCCTCGTTGG-3′
Reverse	5′-CCTCTGTGGAAGGAGAGCAC-3′
MMP2	
Forward	5′-GGACAGTGACACCACGTGAC-3′
Reverse	5′-GTATCCTCGCTCCAGAGTGC-3′
MMP9	
Forward	5′-CATTCGCGTGGATAAGGAGT-3′
Reverse	5′-ACCTGGTTCACCTCATGGTC-3′
β-actin	
Forward	5′-CCTGTATGCCTCTGGTCGTA-3′
Reverse	5′-CCATCTCCTGCTCGAAGTCT-3′

TIMP-1, tissue inhibitor of metalloproteinase-1; MMP, matrix metalloproteinase.

are shown in Table 1. These primers, except those for TIMP-1,[11,14] were designed according to the full-length cDNA sequence in GenBank and their specificity was confirmed by BLAST (National Library of Medicine, Bethesda, MD, USA).

Real-time PCR was performed using a DyNAmo SYBR Green qPCR Kit (Finnzymes, Espoo, Finland). Amplification reactions were performed in a final volume of 20 μl containing, 0.5 μM primer mixture and 2 μl cDNA. The PCR conditions consisted of an initial denaturation step at 95°C for 10 min and 40 cycles at 95°C for 10 s of denaturation, 60°C (collagen type I and type III, TIMP-1, MMP1, and β-actin) or 64°C (MMP2 and MMP9) for 20 s of annealing, and 72°C for 20 s of extension. Each PCR thermal cycle condition was optimized by 1.5% agarose gel electrophoresis to achieve a single band of the expected size. All PCR reactions were performed using an Opticon continuous fluorescence detection system (MJ Research Inc., Waltham, MA, USA). The comparative cycle threshold (Ct) was calculated for all samples to quantify the relative expression of each mRNA with standardization using that of β-actin mRNA. Experiments were performed in duplicate for each data point.

Statistical Analysis

Values are expressed as mean ± SEM. Data were analyzed using ANOVA. If a statistically significant effect was found, *post hoc* analysis was performed to identify the difference between the groups. A value of $p < 0.05$ was considered to be statistically significant.

RESULTS

Cell Infiltration in Subconjunctival Space After Injury Induced by Blunt Dissection

First, we examined the changes in cell infiltration in the subconjunctival space after blunt dissection using WT, $AT_{1a}KO$, and AT_2KO mice. Figure 1 shows the histological changes in the subconjunctival space after operation. Infiltration of mononuclear cells into the subconjunctival space was increased 7- to 10-fold at 1 and 2 days after injury in all groups (Figs. 1a and 1b). The change in cell number was not significantly different among the three groups until 7 days after operation. The cell number at 14 days was significantly greater in AT_2KO mice (Fig. 1b), while it appeared to be smaller in $AT_{1a}KO$ mice. Infiltrating cells in the subconjunctival space after blunt dissection included macrophages and myofibroblasts. As shown in Figure 2, the number of macrophages and myofibroblasts was markedly increased in the subconjunctival space at 2 days after operation. This increase was significantly smaller in $AT_{1a}KO$ mice. In contrast, the increase in myofibroblast number was further enhanced in AT_2KO mice. This enhanced response was observed even at 14 days after operation (Fig. 2b).

Expression of AT_1 and AT_2 Receptors in Subconjunctival Space After Blunt Dissection

Figure 3 shows immunofluorescent staining of AT_1 and AT_2 receptors in the subconjunctival space in sham-operated and injured mice at 2 days after operation. In sham-operated mice, expression of AT_2 receptors was not observed in the subconjunctival space, where there was no apparent cell infiltration. Expression of AT_1 and AT_2 receptors was increased after operation. Both AT_1 and AT_2 receptors were coexpressed in mononuclear cells in the subconjunctival space after operation.

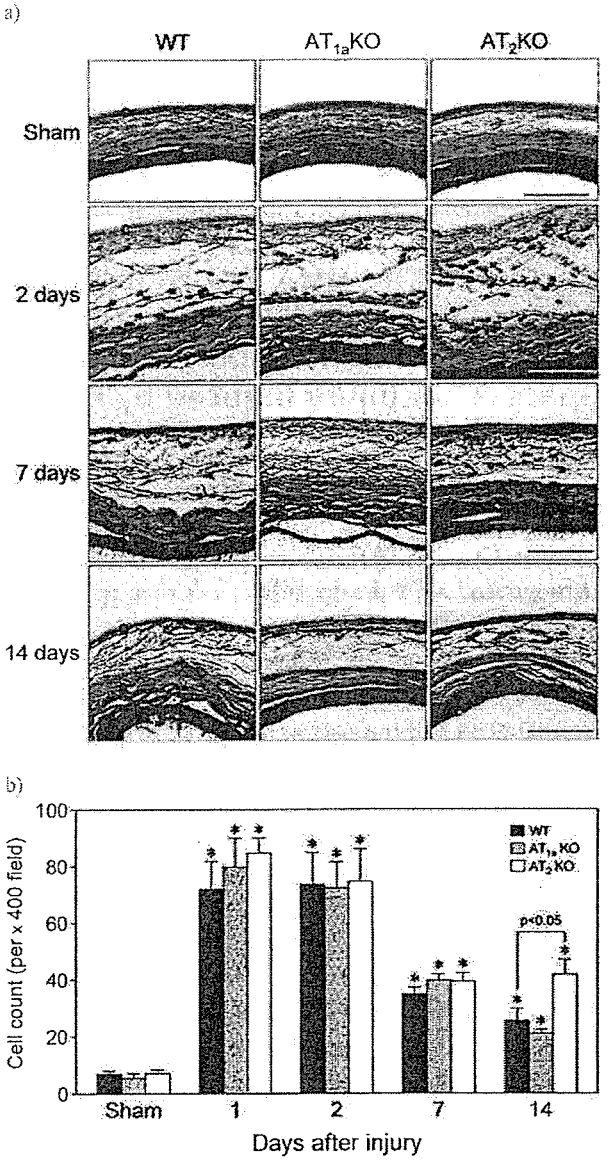

FIGURE 1 Histological changes in subconjunctival tissue in AT_2KO and $AT_{1a}KO$ mice after subconjunctival injury. Subconjunctival injury was induced and cross sections of eye samples were prepared as described in "Materials and Methods." (a) Representative cross sections of injured eyes with hematoxylin and eosin staining. (C, conjunctiva; S, sclera. Magnification, ×400; scale bar, 50 μm.) (b) Changes in total cell count in subconjunctival space after injury. Total cells in the subconjunctival space were counted using a cross section of the eye as described in "Materials and Methods." (Sham, sham operation.) $^*p < 0.05$ versus sham group. Values are mean ± SEM of 4 to 6 animals.

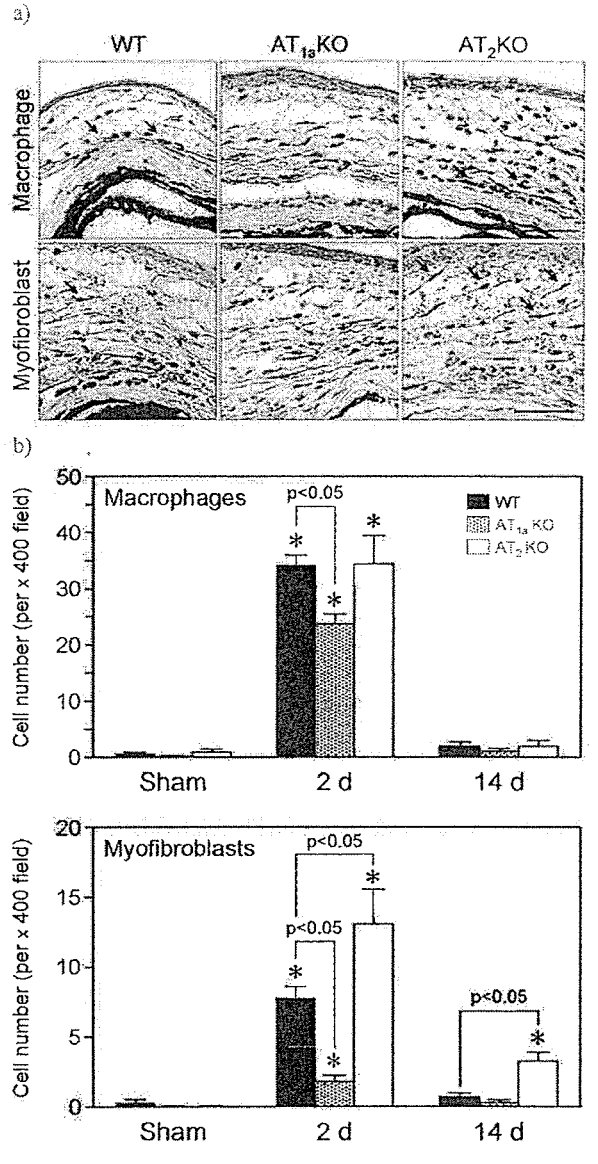

FIGURE 2 Infiltration of macrophages and myofibroblasts into subconjunctival space at 2 days after injury in AT_2KO and $AT_{1a}KO$ mice. Subconjunctival injury was induced and cross sections of eye samples were prepared as described in Figure 1. (a) Immunostaining of macrophages and myofibroblasts in subconjunctival tissue with anti-F4/80 antibody and anti-α-smooth muscle (α-SM) actin antibody, respectively. Arrows show positive staining of each marker. Magnification, ×400; scale bar, 50 μm.) (b) Changes in macrophages and myofibroblasts in subconjunctival tissue. (Sham, sham operation.) Values are mean ± SEM from 4 to 6 animals. $^*p < 0.05$ versus sham group.

Collagen Deposition in Subconjunctival Space After Blunt Dissection

Subconjunctival injury induced an increase in collagen deposition during the wound-healing process. As shown in Figure 4, collagen deposition became apparent at 14 days after operation. This increase in collagen deposition was suppressed in $AT_{1a}KO$ mice, whereas it was further enhanced in AT_2KO mice (fibrosis score was 1.6 ± 0.2, 0.6 ± 0.2, and 2.7 ± 0.3 for WT, $AT_{1a}KO$, and AT_2KO mice, respectively). Figures 5a and 5b show the

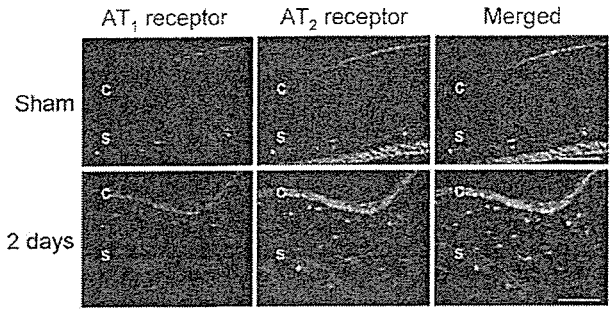

FIGURE 3 Immunofluorescence staining of AT_1 and AT_2 receptors in subconjunctival space at 2 days after injury in WT mice. Subconjunctival injury was induced and cross sections of eye samples were prepared as described in Figure 1. AT_1 and AT_2 receptors were stained using specific antibodies and fluorescent dye Cy3 (red) for AT_1 receptor and FITC (green) for AT_2 receptor, respectively, as described in "Materials and Methods." (C, conjunctiva; S, sclera; Sham, sham operation. Magnification, ×400, scale bar, 50 μm.)

expression of mRNA for collagen type I and type III in injured tissue after blunt dissection of the subconjunctiva. The mRNA levels of collagen type I and type III were markedly increased at 7 days after operation. The increase in collagen type III mRNA was significantly inhibited in AT_{1a}KO mice. In contrast, it was further enhanced in AT_2KO mice. Moreover, the increase in collagen type III mRNA was also enhanced in AT_2KO mice (Fig. 5b).

We also studied the expression of TIMP and MMP in injured tissue after operation (Figs. 5c–5f). Expression of TIMP was markedly increased at 12 hr after operation (Fig. 5c) and then decreased over the next 7 days. The increase in TIMP expression was significantly suppressed in AT_{1a}KO mice during first 24 hr after operation. However, it was further enhanced in AT_2KO mice, and this enhancement of TIMP expression was still observed at 7 days after operation. Among MMP subclasses, expression of MMP1 and MMP9 was not significantly altered after operation in all strains (Figs. 5e and 5f). However, expression of MMP2 was decreased during the first 24 hr after operation in all groups (Fig. 5d). MMP2 expression then recovered to the basal level in WT and AT_2KO mice, while it was significantly greater in AT_{1a}KO mice than in WT mice at 14 days after operation.

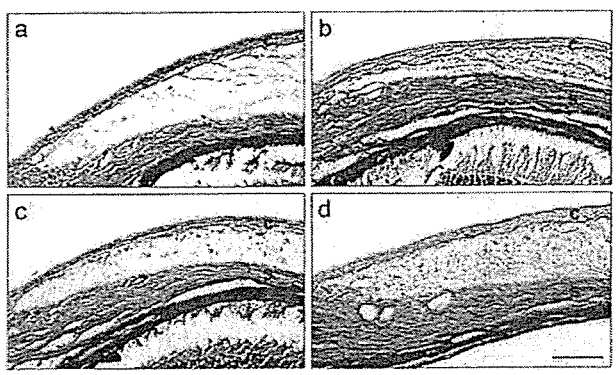

FIGURE 4 Changes in collagen deposition in subconjunctival space at 14 days after injury in sham operation (a), WT (b), AT_{1a}KO (c), and AT_2KO (d) mice. Subconjunctival injury was induced and cross sections of eye samples were prepared as described in Figure 1. Representative results of Elastica van Gieson staining of cross sections of injured eyes. n = 4 to 6. (C, conjunctiva; S, sclera. Magnification, ×400, scale bar, 50 μm.)

DISCUSSION

In the current study, we developed an animal model of subconjunctival injury according to the method of Reichel et al.[13] We used blunt dissection of the subconjunctiva with a spatula instead of injection of phosphate-buffered saline. Our model induced reproducible wound-healing responses, including inflammatory cell infiltration and collagen accumulation in the subconjunctival space. Using this model of subconjunctival damage, we investigated the role of Ang II receptor subtypes in the wound-healing process after ocular injury using receptor gene–deficient mice. Our results indicated that Ang II receptor stimulation is involved in the process of wound healing. It was suggested that AT_{1a} and AT_2 receptors affect wound-healing responses, such as inflammation and collagen deposition, antagonistically through regulation of MMP activity.

It is suggested that wound-healing responses include three phases; inflammation, proliferation, and remodeling.[15] These reactions are also involved in wound healing of conjunctival injury.[13] Previous reports indicated that Ang II plays an important role in the wound-healing process and tissue remodeling in various types of injury.[5–7] The receptor for Ang II has two distinct subtypes named AT_1 and AT_2 receptors.[16,17] In rodents, the AT_1 receptor is divided into two subclasses, AT_{1a} and AT_{1b}.[18] In our study, infiltration of macrophages and myofibroblasts into the subconjunctival space was also observed after subconjunctival blunt dissection. The rest of the cells in the injured tissue seemed to be neutrophils and other mononuclear cells. Such inflammatory responses were reduced in AT_{1a}KO mice, whereas the infiltration of myofibroblasts was significantly enhanced in AT_2KO mice (Fig. 2). Because the AT_{1a} receptor is a major subclass of AT_1 receptor,[4]

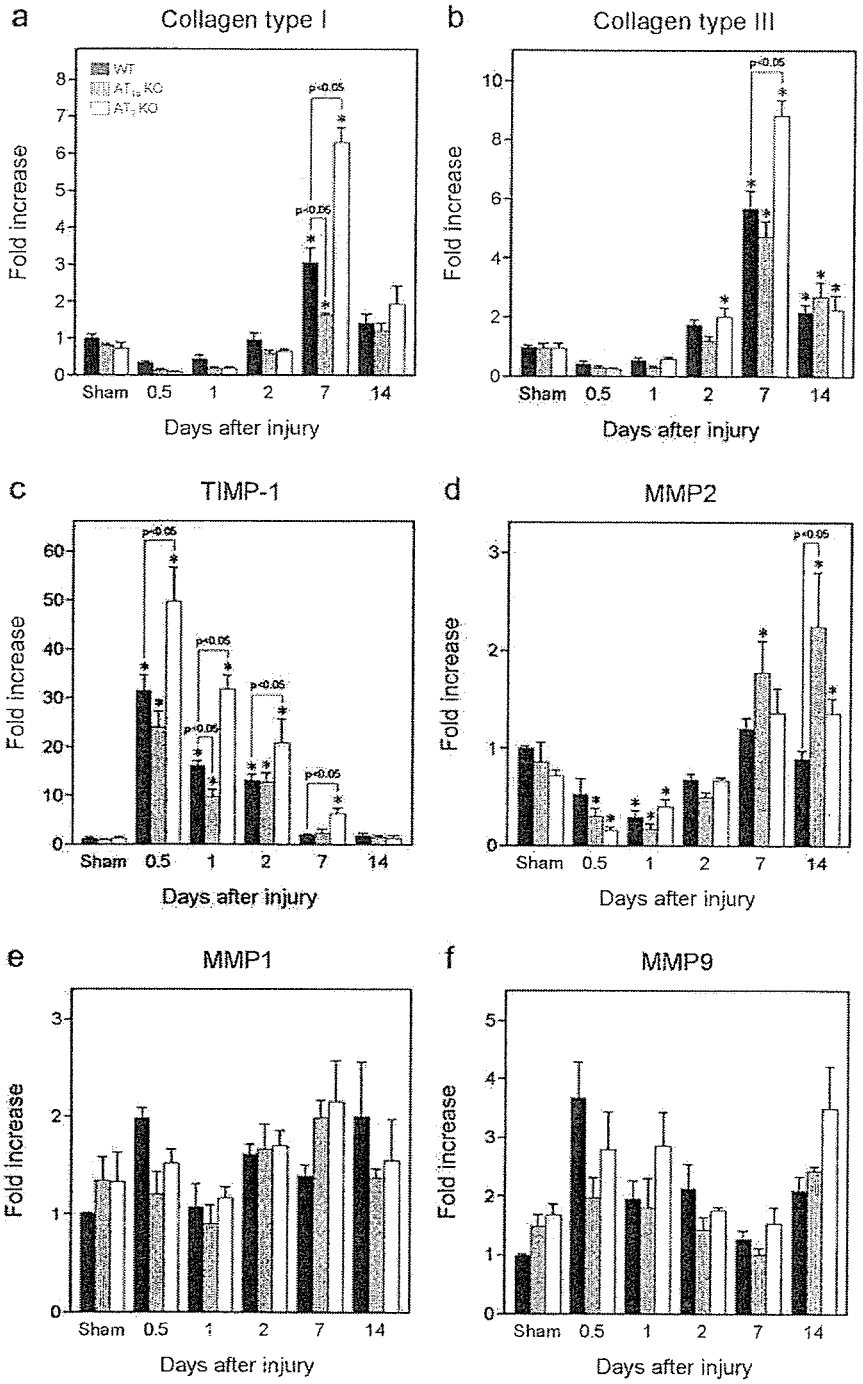

FIGURE 5 Expression of collagen type I (a), collagen type III (b), TIMP-1 (c), MMP2 (d), MMP1 (e), and MMP9 (f). Subconjunctival injury was induced and RNA samples were prepared as described in "Materials and Methods." Real-time PCR was performed as described in "Materials and Methods." mRNA levels were standardized using that of β-actin and expressed as the relative amount in WT mice of the sham group. (Sham, sham operation.) *$p < 0.05$ versus Sham. Values are mean ± SEM of 6 to 9 samples.

these results indicate that Ang II plays an important role in inflammatory responses in subconjunctival injury, and suggest that AT_1 and AT_2 receptors have antagonistic actions on regulation of the wound-healing process.

Myofibroblasts as well as fibroblasts play an important role in collagen synthesis and fibrosis during wound healing.[9,19] Cleutjens et al. reported that myofibroblasts are responsible for the increase in expression of genes

encoding fibrillar type I/III procollagens.[20] It has been demonstrated that collagen production is accelerated by transforming growth factor (TGF)-β1,[21] and Ang II stimulated TGF-β1 production in fibroblasts.[19,22,23] Desmouliere et al.[24] reported that TGF-β1 induced α-SM actin expression in myofibroblasts, thereby inducing differentiation of fibroblasts into myofibroblasts. It has been reported that both TGF-β1 and β2 are activated in mouse subconjunctival tissue after surgical intervention.[25] In addition, Campbell[26] reported that an AT_1 receptor antagonist, losartan, greatly attenuated Ang II–stimulated TGF-β1 secretion in cardiac myofibroblasts. In our study, both AT_1 and AT_2 receptors were expressed in mononuclear cells infiltrating the subconjunctival space in the early phase after injury in WT mice. These results led to the hypothesis that AT_1 and AT_2 receptors regulate fibroblast activation antagonistically through TGF secretion. We have previously demonstrated that Ang II increased collagen production via the AT_1 receptor but inhibited it via the AT_2 receptor in skin fibroblasts.[11] Moreover, AT_1 receptor stimulation enhanced collagen synthesis induced by IGF-1, whereas AT_2 receptor activation inhibited it. Consistent with these results, in the current study the level of mRNA for type 1 collagen was significantly higher in AT_2KO mice but lower in AT_{1a}KO mice than in WT mice. These results suggest that the AT_1 and AT_2 receptors antagonistically regulate collagen synthesis.

It has been reported that matrix metalloproteinases (MMPs), zinc-containing Ca^{2+}-dependent endopeptidases, regulate tissue remodeling by digesting the extracellular matrix (ECM)[27] and that Ang II reduced the activity of MMP2 as well as its protein level, and these effects were inhibited by selective AT_1 receptor blockers.[28] We thus examined MMP mRNA expression in the injured subconjunctiva (Figs. 5d–5f). MMP2 mRNA was decreased during the first 24 hr after operation in all groups. The mRNA level was then recovered to the basal level in WT and AT_2KO mice but further increased in AT_{1a}KO mice. These observations suggest the possibility that AT_1 receptor stimulation causes ECM degradation, which should be clarified in future experiments.

TIMPs are known to be major endogenous inhibitors of MMPs. Four homologous TIMPs, named TIMP-1 to TIMP-4, have been identified and they similarly inhibit MMPs.[27] Especially, TIMP-1 plays an mportant role in the mouse eye.[29–31] In the current study, TIMP-1 expression was significantly lower in AT_{1a}KO mice but higher in AT_2KO mice than in WT mice in the early phase after injury (Fig. 5c). Interestingly, our group has reported that TIMP-1 expression is increased by AT_1 receptor stimulation but decreased by AT_2 receptor stimulation in mouse neonatal skin fibroblasts.[11] In accordance with our results, Chua et al.[32] reported that Ang II induced TIMP-1 production in rat endothelial cells. These results suggest that AT_1 receptor stimulation increases collagen accumulation in subconjunctival fibroblasts, at least in part, by inhibition of collagen degradation via an increase in TIMP-1 expression, whereas AT_2 receptor stimulation inhibits TIMP-1 expression, increases collagen degradation, and thereby inhibits collagen accumulation. Our group also reported that transfection of dominant negative SHP-1 (Src homology 2–containing protein-tyrosine phosphatase-1) mutant inhibited the Ang II–mediated inhibitory effect on both collagen synthesis and TIMP-1 expression in fibroblasts from AT_{1a} KO mice.[11] However, the addition of a serine/threonine phosphatase inhibitor, okadaic acid, did not affect collagen production induced by Ang II.[11] These results suggest that SHP-1 plays a pivotal role in the action of the AT_2 receptor on collagen metabolism.

In summary, we have demonstrated that the wound-healing process with collagen accumulation after ocular injury is regulated by Ang II through antagonistic actions between AT_1 and AT_2 receptors. Our results provide an insight into the pathophysiological significance of tissue Ang II in subconjunctival scarring.

ACKNOWLEDGMENTS

This work was supported by Grants-in-Aid for Scientific Research 14370559 and 15390247 from the Ministry of Education, Science, Sports and Culture of Japan, a grant from the Mitsubishi Pharma Research Foundation, and a grant from the Smoking Research Foundation.

REFERENCES

[1] Lama PJ, Fechtner RD. Antifibrotics and wound healing in glaucoma surgery. *Surv Ophthalmol.* 2003;48:314–346.
[2] Tseng SH, Chen YT, Cheng HC, et al. Impression cytology study of conjunctival epithelial phenotypes on the healing ocular surface after pterygium excision. *Cornea.* 2001;20:244–250.
[3] Tseng SC. Amniotic membrane transplantation for ocular surface reconstruction. *Biosci Rep.* 2001;21:481–489.
[4] de Gasparo M, Catt KJ, Inagami T, et al. International Union of Pharmacology. XXIII. The angiotensin II receptors. *Pharmacol Rev.* 2000;52:415–472.

[5] Rodgers KE, DeCherney AH, St Amand KM, et al. Histologic alterations in dermal repair after thermal injury effects of topical angiotensin II. *J Burn Care Rehabil.* 1997;18:381–388.
[6] Okuyama N, Roda N, Sherman R, et al. Angiotensin II improves random-flap viability in a rat model. *Ann Plast Surg.* 1999;42:313–319.
[7] Rodgers KE, Roda N, Felix JE, et al. Histological evaluation of the effects of angiotensin peptides on wound repair in diabetic mice. *Exp Dermatol.* 2003;12:784–790.
[8] Gabbiani G. The myofibroblast: a key cell for wound healing and fibrocontractive diseases. *Prog Clin Biol Res.* 1981;54:183–194.
[9] Sun Y, Weber KT. Angiotensin converting enzyme and myofibroblasts during tissue repair in the rat heart. *J Mol Cell Cardiol.* 1996;28:851–858.
[10] Nakajima M, Hutchinson HG, Fujinaga M, et al. The angiotensin II type 2 (AT2) receptor antagonizes the growth effects of the AT1 receptor: gain-of-function study using gene transfer. *Proc Natl Acad Sci USA.* 1995;92:10663–10667.
[11] Min LJ, Cui TX, Yahata Y, et al. Regulation of collagen synthesis in mouse skin fibroblasts by distinct angiotensin II receptor subtypes. *Endocrinology.* 2004;145:253–260.
[12] Ramirez M, Davidson EA, Luttenauer L, et al. The renin-angiotensin system in the rabbit eye. *J Ocul Pharmacol Ther.* 1996;12:299–312.
[13] Reichel MB, Cordeiro MF, Alexander RA, et al. New model of conjunctival scarring in the mouse eye. *Br J Ophthalmol.* 1998;82:1072–1077.
[14] Madlener M, Parks WC, Werner S. Matrix metalloproteinases (MMPs) and their physiological inhibitors (TIMPs) are differentially expressed during excisional skin wound repair. *Exp Cell Res.* 1998;242:201–210.
[15] Kirsner RS, Eaglstein WH. The wound healing process. *Dermatol Clin.* 1993;11:629–640.
[16] Whitebread S, Mele M, Kamber B, de Gasparo M. Preliminary biochemical characterization of two angiotensin II receptor subtypes. *Biochem Biophys Res Commun.* 1989;163:284–291.
[17] Chiu AT, Herblin WF, McCall DE, et al. Identification of angiotensin II receptor subtypes. *Biochem Biophys Res Commun.* 1989;165:196–203.
[18] Burson JM, Aguilera G, Gross KW, Sigmund CD. Differential expression of angiotensin receptor 1A and 1B in mouse. *Am J Physiol.* 1994;267:E260–E267.
[19] Lee AA, Dillmann WH, McCulloch AD, Villarreal FJ. Angiotensin II stimulates the autocrine production of transforming growth factor-beta 1 in adult rat cardiac fibroblasts. *J Mol Cell Cardiol.* 1995;27:2347–2357.
[20] Cleutjens JP, Verluyten MJ, Smiths JF, Daemen MJ. Collagen remodeling after myocardial infarction in the rat heart. *Am J Pathol.* 1995;147:325–338.
[21] Butt RP, Laurent GJ, Bishop JE. Collagen production and replication by cardiac fibroblasts is enhanced in response to diverse classes of growth factors. *Eur J Cell Biol.* 1995;68:330–335.
[22] Sadoshima J, Izumo S. Molecular characterization of angiotensin II-induced hypertrophy of cardiac myocytes and hyperplasia of cardiac fibroblasts. Critical role of the AT1 receptor subtype. *Circ Res.* 1993;73:413–423.
[23] Fisher SA, Absher M. Norepinephrine and ANG II stimulate secretion of TGF-beta by neonatal rat cardiac fibroblasts in vitro. *Am J Physiol.* 1995;268:C910–C917.
[24] Desmouliere A, Geinoz A, Gabbiani F, Gabbiani G. Transforming growth factor-beta 1 induces alpha-smooth muscle actin expression in granulation tissue myofibroblasts and in quiescent and growing cultured fibroblasts. *J Cell Biol.* 1993;122:103–111.
[25] Mietz H, Chevez-Barrios P, Lieberman MW. A mouse model to study the wound healing response following filtration surgery. *Graefes Arch Clin Exp Ophthalmol.* 1998;236:467–475.
[26] Campbell SE, Katwa LC. Angiotensin II stimulated expression of transforming growth factor-beta1 in cardiac fibroblasts and myofibroblasts. *J Mol Cell Cardiol.* 1997;29:1947–1958.
[27] Gomez DE, Alonso DF, Yoshiji H, Thorgeirsson UP. Tissue inhibitors of metalloproteinases: structure, regulation and biological functions. *Eur J Cell Biol.* 1997;74:111–122.
[28] Peng J, Gurantz D, Tran V, et al. Tumor necrosis factor-alpha-induced AT1 receptor upregulation enhances angiotensin II-mediated cardiac fibroblast responses that favor fibrosis. *Circ Res.* 2002;91:1119–1126.
[29] Yang YN, Bauer D, Wasmuth S, et al. Matrix metalloproteinases (MMP-2 and 9) and tissue inhibitors of matrix metalloproteinases (TIMP-1 and 2) during the course of experimental necrotizing herpetic keratitis. *Exp Eye Res.* 2003;77:227–237.
[30] Kernacki KA, Barrett R, Hazlett LD. Evidence for TIMP-1 protection against P. aeruginosa-induced corneal ulceration and perforation. *Invest Ophthalmol Vis Sci.* 1999;40:3168–3176.
[31] Majka S, McGuire P, Colombo S, Das A. The balance between proteinases and inhibitors in a murine model of proliferative retinopathy. *Invest Ophthalmol Vis Sci.* 2001;42:210–215.
[32] Chua CC, Hamdy RC, Chua BH. Angiotensin II induces TIMP-1 production in rat heart endothelial cells. *Biochim Biophys Acta.* 1996;1311:175–180.